Metal Hydride Storage Tank State of Charge Estimation: A Switched Observer Approach

Mingrui Chen, Andreu Cecilia, *Member, IEEE*, Jing Na, *Member, IEEE*, Carles Batlle and Ramon Costa-Castelló, *Senior Member, IEEE*,

***Abstract*—State of charge is an important indicator for metal hydride storage tanks monitoring and operation. This indicator cannot be directly measured, which motivates the design of real-time estimators. Nonetheless, the development of model-based estimators is a non-trivial task for this system, since metal hydride storage tanks dynamics are characterized by being nonlinear and hybride. To overcome these difficulties, this work proposes a novel nonlinear switched observer for a metal hydride storage tank system. Based on differential detectability and recent results on contraction theory for switched systems, we present sufficient conditions for the convergence of the observer under the assumption that the observer and the plant have synchronized switching. Additionally, to guarantee this synchronization, we propose an unknown system dynamics estimator to determine the current system mode. The algorithm is then validated in a set of numerical simulations and in an experimental prototype.**

***Index Terms*—Metal hydride storage tank, Nonlinear observer, State of charge (SOC), Differential detectability, Switched system**

I. Introduction

SOLID-state hydrogen storage is a prospective hydrogen storage technology due to its potential of high hydrogen densities at moderate temperature and pressure levels [1], [2]. Metal hydride (MH) hydrogen storage tanks have received a wide range of attention as an important container for solid-state hydrogen storage due to the slow and controlled rate of hydrogen release from the metal hydrides that fill the tanks, which provide a steady supply of hydrogen [3], [4].

In MH tanks, during a charge process, hydrogen enters the tank from the outlet and reacts with the metal alloy to form metal hydride, while, during a discharge process, the metal hydride releases the stored hydrogen [5]. A general scheme of a MH tank can be found in Fig. 1. The maximum capacity of the MH tank is a fixed value, thus overfilling the tank with hydrogen would cause safety issues. Consequently, it is crucial to monitor in real-time the amount of hydrogen stored in the tank. This quantity is defined as the state of charge (SOC) of the system.

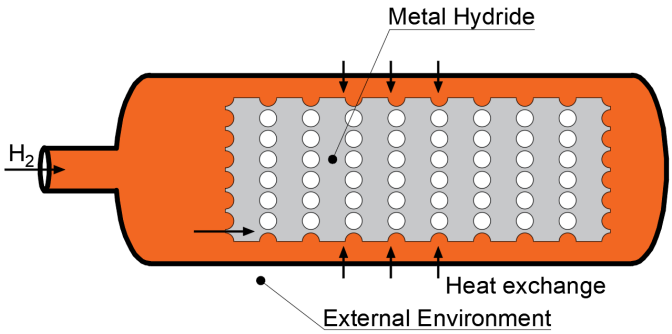

Fig. 1. General scheme of a MH tank

However, real-time estimation of SOC remains a great challenge due to the strong nonlinearity of MH tanks. Suárez et al. [6] estimated the mass of hydrogen absorbed or desorbed through an open-loop integration of the flow rate. Nonetheless, this approach can only be used to estimate the remaining hydrogen mass of the tanks when the initial hydrogen mass is precisely known. In addition, the direct integration of the flow signal is highly sensitive to sensor noise, while the cumulative error introduced over long periods of monitoring has a non-negligible effect on the results. Chabane et al. [7] proposed an alternative method for estimating the SOC of MH tanks by applying piezoelectric materials, the essence of which is to establish a link between the voltage of the piezoelectric material and the equilibrium pressure of the tanks, whereas the relationship between the equilibrium pressure and the SOC can be represented by the Pressure-Composition-Temperature (PCT) curve, so that the SOC of MH tanks can be estimated from the voltage of the piezoelectric material. The limitation of this method is that the SOC can only be estimated for MH tanks in equilibrium and not for MH tanks that are being charged or discharged, which limits the application in most practical situations. A real-time SOC estimation method was proposed in [8], Zhu et al. designed a joint multi-classifier to identify the state of the MH tank, which was subsequently combined with the SOC model to calculate the SOC of the MH tank in real-time. However, to train the joint multi-classifier, a large dataset needs to be obtained. In addition,

This work is part of the Project MAFALDA (PID2021-126001OB-C31 funded by MCIN/ AEI /10.13039/50110001 1033 and by "ERDF A way of making Europe") and Project MASHED (TED2021-129927B-I00 funded by MCIN/AEI /10.13039/501100011033 and by the "European Union Next GenerationEU/PRTR"). This work is partially supported by National Natural Science Foundation of China under grant (62273169) and the Chinese Scholarship Council (CSC) under grant (202208530009).

Mingrui Chen is with the Institut de Robòtica i Informàtica Industrial, CSIC-UPC. C/ Llorens i Artigas 4-6, 08028 Barcelona, Spain. (*Email: chenmingrui2018@gmail.com*)

Andreu Cecilia and Ramon Costa-Castelló are with the Universitat Politècnica de Catalunya, Avinguda Diagonal, 647, 08028 Barcelona, Spain. (*Email: andreu.cecilia@upc.edu, ramon.costa@upc.edu*)

Jing Na is with the Faculty of Mechanical and Electrical Engineering, Kunming University of Science and Technology, and also with Yunnan Key Laboratory of Intelligent Control and Application, Kunming, 650500, P.R. China. (*Email: najing25@163.com*)

Carles Batlle is with the Departament de Matemàtiques, Institut d'Organització i Control, EPSEVG, UPC, 08800 Vilanova i la Geltru, Spain. (*Email: carles.batlle@upc.edu*)

the computational cost required to train the classifier is large.

The main objective of this work is to develop a state observer to estimate the hydrogen and MH densities of a MH tank from easily measured signals, then, use these estimations to compute the SOC of the system. This problem presents several challenges that must be taken into account. First, depending on the state of the system, three modes of MH tanks exist: absorption, equilibrium, and desorption [9]. As a consequence, the MH tank model is a switched nonlinear system with state-dependent switching. Second, when the MH tank is in equilibrium, the same pressure may correspond to different MH densities. Therefore, among the three modes of MH tanks, the equilibrium mode is non-observable, that is, the MH tank model is a switched system with mixed observable and non-observable modes. Consequently, although we may be able to design stable observers for each observable mode, proving the stability of the observers remains a challenge when the system can momentarily evolve in the unobservable one.

With this in mind, the specific contributions of this work are as follows:

1) Study the observability properties of the system using the framework of differential detectability [10, Section IV]. Then based on the observability results, a novel switched nonlinear observer for the MH tanks system only using temperature, flow rate and pressure is proposed.
2) Design an estimator for the sorption rate of MH tanks based on the unknown system dynamic estimator (USDE) [11] and provide sufficient conditions for the stability of the architecture based on recent results of contraction analysis for switched systems [12].
3) Validate the observer through numerical simulations and experimental prototype experiment.

The remainder of the paper is organized as follows. Section II introduces the MH tank model, and formulates the observer design and SOC estimation problem to be solved. In Section III, the observability properties of the MH tank are introduced and studied. Section IV proposes the nonlinear observer of the MH tank model. Section V validates the algorithm through two numerical simulations while Section VI validates the technique in a real MH tank test bench. The conclusions are drawn in Section VII.

II. MH TANK MODEL AND PROBLEM FORMULATION

A. Mathematical Model of MH tanks

This paper utilizes the mathematical model of an MH tank experimentally validated in our previous work [13]. Specifically, the model of the MH tank can be depicted in the following state-space form:

$$\dot{\mathbf{x}} = \mathbf{f}(\mathbf{x}, \mathbf{u}) = \begin{bmatrix} \dfrac{u_2 - f_r\left(x_2, u_1, \bar{y}(x_1, u_1)\right)}{v_g} \\ \dfrac{f_r\left(x_2, u_1, \bar{y}(x_1, u_1)\right)}{v_s} \end{bmatrix}, \tag{1}$$

$$\bar{y} = h(\mathbf{x}, \mathbf{u}) = x_1 \frac{u_1 R}{M_{H_2}}. \tag{2}$$

The state vector, $\mathbf{x}$, is defined as: $\mathbf{x} = [x_1, x_2]^\top = [\rho_g, \rho_s]^\top$, where ρ_g [$\mathrm{kg/m^3}$] is the density of hydrogen and ρ_s [$\mathrm{kg/m^3}$] is the density of the metal hydride. The model includes two measurable inputs, $\mathbf{u} = [u_1, u_2]^\top = [t_{tank}, f_{in}]^\top$, being the temperature of the MH tank, t_{tank} [K], and the normalized mass flow rate of hydrogen, f_{in} [$\mathrm{kg/m^3/s}$]. Finally, it is assumed that there is a measurable output, $\bar{y}$, which is the MH tank pressure, p [Pa]. The other parameters are: the universal gas constant, R [$8.314\,\mathrm{J/mol/K}$] and the molar mass of hydrogen, M_{H_2} [$2.016 \times 10^{-3}\,\mathrm{kg/mol}$].

Furthermore, the normalized sorption mass flow rate of hydrogen, f_r, is calculated through the following piece-wise smooth function:

$$\begin{cases} f_{r,a} = c_a e^{-\frac{E_a}{R \cdot t_{tank}}} \ln\left(\frac{p}{p_{eq,a}}\right)(\rho_{ss} - \rho_s), & p > p_{eq,a}, \\ f_{r,d} = c_d e^{-\frac{E_d}{R \cdot t_{tank}}} \left(\frac{p - p_{eq,d}}{p_{eq,d}}\right)(\rho_s - \rho_{s0}), & p < p_{eq,d}, \\ f_{r,e} = 0, & \text{otherwise.} \end{cases} \tag{3}$$

where c_a [$1/\mathrm{s}$] and c_d [$1/\mathrm{s}$] are the absorption and desorption constants, E_a [$\mathrm{J/mol}$] and E_d [$\mathrm{J/mol}$] are the activation energy for absorption and desorption, $p_{eq,a}$ [Pa] and $p_{eq,d}$ [Pa] are the equilibrium pressure for absorption and desorption, respectively. ρ_{ss} [$\mathrm{kg/m^3}$] is the density of the metal hydride when the absorbed hydrogen reaches its saturated density and ρ_{s0} [$\mathrm{kg/m^3}$] is the density of the metal alloy (with no hydrogen).

The equilibrium pressures $p_{eq,a}$ and $p_{eq,d}$ that define the boundaries for the function switching in (3) are computed as

$$p_{eq,a} = p_0 \cdot e^{\left(\frac{\Delta S_d}{R} - \frac{\Delta H_d}{R \cdot t_{tank}} + (\varphi + \varphi_0)\tan\left[\pi\left(\frac{\rho_s - \rho_{s0}}{\rho_{ss} - \rho_{s0}} - 0.5\right)\right] + \frac{\beta}{2}\right)}, \tag{4}$$

$$p_{eq,d} = p_0 \cdot e^{\left(\frac{\Delta S_d}{R} - \frac{\Delta H_d}{R \cdot t_{tank}} + (\varphi - \varphi_0)\tan\left[\pi\left(\frac{\rho_s - \rho_{s0}}{\rho_{ss} - \rho_{s0}} - 0.5\right)\right] - \frac{\beta}{2}\right)}, \tag{5}$$

where p_0 [Pa] is the atmospheric pressure, ΔH_d [$\mathrm{J/mol}$] and ΔS_d [$\mathrm{J/mol/K}$] are the enthalpy change and the entropy change for desorption, respectively. φ [-] and φ_0 [-] are the plateau flatness coefficients, β [-] is the plateau hysteresis coefficient.

Finally, the saturated density ρ_{ss} is computed as

$$\rho_{ss} = \rho_{s0} + \frac{v_{H_2} \cdot \rho_{H_2}}{v_{MH} \cdot (1 - \epsilon)} \tag{6}$$

where v_{H_2} [$\mathrm{m^3}$] is the capacity of hydrogen that can be absorbed by the tank, and ρ_{H_2} [$\mathrm{kg/m^3}$] is the density of hydrogen ($1\,\mathrm{atm}$, $0\,^\circ\mathrm{C}$), which is considered a constant. v_{MH} [$\mathrm{m^3}$] and ε are the volume and porosity of the metal hydride.

B. Main objective

The main objective of this paper is to estimate the state of the MH tank model, that is, the densities of hydrogen and MH. In particular, we will solve this problem by means of a nonlinear observer that uses the temperature, pressure and flow rate as measured signals. Subsequently, the SOC of the MH tank can computed from the obtained estimations. Precisely, the SOC of the MH tank can be computed through the following equation [8]:

$$soc_{tank} \triangleq \frac{m_{H_2}}{m_{total}}, \tag{7}$$

where m_{H_2} [kg] is the current hydrogen amount and m_{total} [kg] is the maximum hydrogen capacity of the MH tank.

From (1), it can be noted that $v_s\dot{x}_2+v_g\dot{x}_1 = u_2$, so m_{H_2} can be calculated from the initial hydrogen mass and the integral of flow rate:

$$\begin{aligned} m_{H_2}(t) &= m_{H_2}(0) + v_{MH}\cdot\int_0^t u_2 dt \\ &= m_{H_2}(0) + v_{MH}\cdot v_s\cdot(x_2(t) - x_2(0)) \\ &+ v_{MH}\cdot v_g\cdot(x_1(t) - x_1(0)) \end{aligned} \tag{8}$$

where $x_2(0)$ is the initial density of the metal hydride and $x_1(0)$ is the initial density of the hydrogen, $m_{H_2}(0)$ [kg] is the initial hydrogen mass of the MH tank which can be calculated as:

$$m_{H_2}(0) = v_{MH}\cdot v_s\cdot(x_2(0) - \rho_{s0}) + v_{MH}\cdot v_g\cdot x_1(0). \tag{9}$$

Substituting (9) into (8), we can compute soc_{tank} as

$$soc_{tank} = \frac{v_{MH}v_g}{m_{total}}x_1 + \frac{v_{MH}v_s}{m_{total}}(x_2 - \rho_{s0}). \tag{10}$$

Since the variables x_1 and x_2 in the definition are unknown (all the remaining ones are constants and assumed known) the SOC estimation becomes a problem of estimating the states x_1 and x_2 in real-time. Thus, we convert the problem of estimating the SOC of MH tanks into an observer design problem.

More precisely, the observer design problem can be defined as the problem of finding a dynamic system of the form

$$\dot{\hat{\mathbf{x}}} = \mathbf{j}(\hat{\mathbf{x}}, y, \mathbf{u}), \tag{11}$$

with state $\hat{\mathbf{x}} \in \mathbb{R}^2$ and vector field $\mathbf{j} : \mathbb{R}^2 \times \mathbb{R} \times \mathbb{R}^2 \to \mathbb{R}^2$, such that for all initial conditions $\mathbf{x}(0) \in \mathbb{R}^2$, $\hat{\mathbf{x}}(0) \in \mathbb{R}^2$,

$$\lim_{t\to\infty} \|\mathbf{x}(t) - \hat{\mathbf{x}}(t)\| = 0. \tag{12}$$

Then, the estimation of SOC $\hat{soc}_{tank}$ is

$$\hat{soc}_{tank} = \frac{v_{MH}v_g}{m_{total}}\hat{x}_1 + \frac{v_{MH}v_s}{m_{total}}(\hat{x}_2 - \rho_{s0}). \tag{13}$$

Now, before presenting the main result of the paper, that is, the observer (11), we need to study whether the considered estimation problem can be solved. That is, we need to analyze if the measured signal $\bar{y}$ in (1) contains enough information to uniquely reconstruct the states $\mathbf{x}$. Next section is dedicated to this purpose.

III. Observability properties of the model

A. Preliminaries

Before presenting the structural conditions of system (1), we need to introduce some concepts that will be utilized throughout the work. To simplify the presentation, we consider a generic nonlinear system in which the output map is linear:

$$\begin{aligned} \dot{\mathbf{x}} &= \mathbf{f}(\mathbf{x}, \mathbf{u}) \\ \mathbf{y} &= \mathbf{c}\mathbf{x}, \end{aligned} \tag{14}$$

where $\mathbf{x} \in \mathbb{R}^{n_x}$ is the state vector, $\mathbf{y} \in \mathbb{R}^{n_y}$ is the output vector and $\mathbf{u} \in \mathbb{R}^{n_u}$ is the input vector. Additionally, assume that the vector field $\mathbf{f}$ is sufficiently smooth in its first argument and piecewise-continuous in its second. Moreover, assume that the system (14) is forward invariant and has a unique solution in a compact set $\mathbf{X} \subsetneq \mathbb{R}^{n_x}$ uniformly for all $\mathbf{u} \in \mathbf{U} \subsetneq \mathbb{R}^{n_u}$ where $\mathbf{U}$ is also a compact set.

With this system in mind, we define the concept of differential detectability that will be used throughout the work as follows.

Definition 1 (Differential Detectability [10]): The system (14) *is differentially detectable (with respect to an Euclidean metric) uniformly on the input* $\mathbf{u}$ *if there exists a constant positive definite symmetric matrix* $\mathbf{P} \in \mathbb{R}^{n_x\times n_x}$ *and some constants* $\mu, q > 0$ *such that*

$$\mathbf{P}\frac{\partial \mathbf{f}}{\partial \mathbf{x}}(\mathbf{x}, \mathbf{u}) + \frac{\partial \mathbf{f}}{\partial \mathbf{x}}(\mathbf{x}, \mathbf{u})^\top \mathbf{P} - \mu \mathbf{c}^\top \mathbf{c} \preceq -q\mathbf{P} \tag{15}$$

for all $\mathbf{x} \in \mathbf{X}$ *and* $\mathbf{u} \in \mathbf{U}$.

In plain words, differential detectability implies that for any two trajectories of system (14), denoted as $\mathbf{x}(t)$, $\mathbf{x}'(t)$, in $\mathbf{X}$, indistinguishable from the output, that is $\mathbf{c}\mathbf{x}(t) = \mathbf{c}\mathbf{x}'(t)$ for all $t \geq 0$ with the same input $\mathbf{u} \in \mathbf{U}$, the two indistinguishable trajectories converge asymptotically to each other. For more details on this property, see [10, Section IV].

Remark 1: Differential detectability does not imply that the system is observable. Indeed, differential detectability indicates that trajectories indistinguishable from the output converge to each other, while observability implies that there are no trajectories indistinguishable from the output. The observability condition is stronger compared to differential detectability.

Remark 2: Even though the Jacobian of the vector field appears in (15)*, differential detectability is a global property. Consequently, different to observers based on a linearization as the extended Kalman filter [14], an observer designed according to differential detectability does not require the initial value of the observer to be close to the true value.*

Additionally, we introduce the notion of a non-expansive system, which has also been studied, albeit from a different perspective, in [15].

Definition 2: The system (14) *is non-expansive (with respect to an Euclidean metric) uniformly on the input* $\mathbf{u}$ *if there exists a constant positive definite symmetric matrix* $\mathbf{P} \in \mathbb{R}^{n_x\times n_x}$ *such that*

$$\mathbf{P}\frac{\partial \mathbf{f}}{\partial \mathbf{x}}(\mathbf{x}, \mathbf{u}) + \frac{\partial \mathbf{f}}{\partial \mathbf{x}}(\mathbf{x}, \mathbf{u})^\top \mathbf{P} \preceq 0 \tag{16}$$

for all $\mathbf{x} \in \mathbf{X}$ *and* $\mathbf{u} \in \mathbf{U}$.

A direct consequence of non-expansiveness is that the distance between any pair of trajectories of the system remains bounded. More precisely, for any two trajectories of system (14), denoted as $\mathbf{x}(t)$, $\mathbf{x}'(t)$ in $\mathbf{X}$, there exists a positive constant $a \in \mathbb{R}$ such that for all $t \geq t_0 \geq 0$

$$\|\mathbf{x}(t) - \mathbf{x}'(t)\| \leq a\|\mathbf{x}(t_0) - \mathbf{x}'(t_0)\|. \tag{17}$$

For the case $a = 1$, this definition recovers the one presented in [15] with respect to the Euclidean norm. We also remark that non-expansiveness does not imply that the trajectories converge one to the other.

Non-expansiveness contrasts with the property of contraction, which does actually imply that the trajectories of the

system converge one to the other, and can be defined as follows:

Definition 3: The system (14) *is uniformly contracting if there exists some constants* $a, b > 0$ *such that, for any two trajectories of system* (14)*, denoted as* $\mathbf{x}(t)$*,* $\mathbf{x}'(t)$ *in* $\mathbf{X}$*, and any input* $\mathbf{u} \in \mathbf{U}$ *the following holds for all* $t \geq t_0 \geq 0$

$$\|\mathbf{x}(t) - \mathbf{x}'(t)\| \leq ae^{-b(t-t_0)}\|\mathbf{x}(t_0) - \mathbf{x}'(t_0)\|. \tag{18}$$

More details on this contraction property can be found in [16].

Finally, we end the section by providing, in the following remark, a convex strategy in order to evaluate conditions (15) and (16).

Remark 3: Notice that conditions (15) *and* (16) *require solving a set of infinite matrix inequalities that depend on the state* $\mathbf{x}$ *and input* $\mathbf{u}$*. Nonetheless, we can obtain a finite set of LMIs through convex relaxation, see e.g. [17]. Specifically, let* $\mathcal{A} = \{\mathbf{A}_1, \ldots, \mathbf{A}_N\}$ *be a family of matrices in* $\mathbb{R}^2$ *such that* $\frac{\partial \mathbf{f}}{\partial \mathbf{x}}(\mathbf{x}, \mathbf{u}) \in$ *ConvexHull*$(\mathcal{A})$ *for all* $(\mathbf{x}, \mathbf{u})$*. Then, at each* $(\mathbf{x}, \mathbf{u})$ *we have that* $\frac{\partial \mathbf{f}}{\partial \mathbf{x}}(\mathbf{x}, \mathbf{u}) = \sum_{i=1}^{N} \varrho_i(\mathbf{x}, \mathbf{u})\mathbf{A}_i$*, for some* $\varrho_i(\mathbf{x}, \mathbf{u})$ *such that* $\sum_{i=1}^{N} \varrho_i(\mathbf{x}, \mathbf{u}) = 1$ *for all* $(\mathbf{x}, \mathbf{u})$*. With this in mind, inequality* (15) *reads as*

$$\sum_{i=1}^{N} \varrho_i(\mathbf{x}, \mathbf{u}) \left(\mathbf{P}\mathbf{A}_i + \mathbf{A}_i^\top \mathbf{P} - \mu \mathbf{c}^\top \mathbf{c}\right) \preceq -q\mathbf{P}.$$

Consequently, any symmetric positive definite matrix $\mathbf{P}$ *that is a solution of*

$$\mathbf{P}\mathbf{A}_i + \mathbf{A}_i^\top \mathbf{P} - \mu \mathbf{c}^\top \mathbf{c} \preceq -q\mathbf{P}, \quad i = 1, \ldots, N$$

is also a solution of (15)*. Then,* (16) *can be analyzed similarly.*

With these definitions in mind, we proceed by analysing the structural properties of the MH tank model (1) and (2).

B. Observability analysis

Before presenting the analysis, we will slightly reformulate the MH tank model (1)-(2). First, it can be noted that the output of the original system presents a bilinear term on x_1 and u_1. For this reason, we introduce the following transformation linearizes the output (2)

$$y = \bar{y}\frac{M_{H_2}}{u_1 R} = \mathbf{c}\mathbf{x} = \begin{bmatrix} 1 & 0 \end{bmatrix} \mathbf{x}. \tag{19}$$

Since u_1 is a strictly positive quantity, this transformation is always well defined.

Second, considering the piece-wise function in (3), the whole $\mathbb{R}^2$ can be divided into the following three subsets

$$\begin{cases} \Omega_1 : \left\{\mathbf{x} \in \mathbb{R}^2, \mathbf{u} \in \mathbb{R}^2 \,|\, p > p_{eq,a}\right\}, \\ \Omega_2 : \left\{\mathbf{x} \in \mathbb{R}^2, \mathbf{u} \in \mathbb{R}^2 \,|\, p_{eq,a} \leq p \leq p_{eq,d}\right\}, \\ \Omega_3 : \left\{\mathbf{x} \in \mathbb{R}^2, \mathbf{u} \in \mathbb{R}^2 \,|\, p < p_{eq,d}\right\}. \end{cases} \tag{20}$$

Then, the original MH tank model can be rewritten as the following switched system:

$$\begin{aligned} \dot{\mathbf{x}} &= \mathbf{f}_\sigma(\mathbf{x}, \mathbf{u}), \\ y &= \mathbf{c}\mathbf{x} = \begin{bmatrix} 1 & 0 \end{bmatrix} \mathbf{x}, \end{aligned} \tag{21}$$

Table I: Parameters of the MH tank model used in differential detectability analysis

Symbol	Value	Symbol	Value
ϵ	0.6992	v_{MH}	$0.353 \times 10^{-3}\,\mathrm{m}^3$
ρ_{s0}	$6350\,\mathrm{kg/m}^3$	ρ_{H_2}	$0.0897\,\mathrm{kg/m}^3$
R	$8.314\,\mathrm{J/(mol \cdot K)}$	p_0	$101\,325\,\mathrm{Pa}$
M_{H_2}	$2.016 \times 10^{-3}\,\mathrm{kg/mol}$	v_{H_2}	$0.35\,\mathrm{m}^3$
v_{tank}	$0.48 \times 10^{-3}\,\mathrm{m}^3$	ΔS_d	$112.3193\,\mathrm{J/mol/K}$
ΔH_d	$2.6967 \times 10^4\,\mathrm{J/mol}$	φ	0.1770
φ_0	0.0030	β	0.2779
c_a	$843.5713\,1/\mathrm{s}$	c_d	$3109.0\,1/\mathrm{s}$
E_a	$3.2573 \times 10^4\,\mathrm{J/mol}$	E_d	$3.3151 \times 10^4\,\mathrm{J/mol}$

where σ is a switching signal for system dynamics $\mathbf{f}$ with the index set $\mathcal{G} \coloneqq \{1, 2, 3\}$ that is equal to p when $(\mathbf{x}, \mathbf{u}) \in \Omega_p$. The vector field $\mathbf{f}_p$ with $p \in \mathcal{G}$ is defined as

$$\begin{aligned} \mathbf{f}_1(\mathbf{x}, \mathbf{u}) &= \begin{bmatrix} \dfrac{u_2 - f_{r,a}(x_2, u_1, x_1)}{v_g} \\ \dfrac{f_{r,a}(x_2, u_1, x_1)}{v_s} \end{bmatrix}, \\ \mathbf{f}_2(\mathbf{x}, \mathbf{u}) &= \begin{bmatrix} \dfrac{u_2}{v_g} \\ 0 \end{bmatrix}, \\ \mathbf{f}_3(\mathbf{x}, \mathbf{u}) &= \begin{bmatrix} \dfrac{u_2 - f_{r,d}(x_2, u_1, x_1)}{v_g} \\ \dfrac{f_{r,d}(x_2, u_1, x_1)}{v_s} \end{bmatrix}. \end{aligned} \tag{22}$$

With this reformulation, we can now present the structural properties of the model in each subset defined in (20). We first consider the pressure equilibrium case, i.e. $\mathbf{f} = \mathbf{f}_2$. In this subset, we have that, for all $(\mathbf{x}, \mathbf{u}) \in \Omega_2$,

$$\frac{\partial \mathbf{f}_2}{\partial \mathbf{x}}(\mathbf{x}, \mathbf{u}) = 0. \tag{23}$$

Consequently, it is trivial to see that the MH tank model satisfies (16) for any positive and symmetric matrix $\mathbf{P}$, thus, is non-expansive in region Ω_2 with $a = 1$. Besides, the model does not satisfy any detectability and/or observability property in this region, since the vector field of the model is independent of the states and $\mathbf{c}$ is not invertible.

Next, we consider the absorption and desorption cases, that is, regions Ω_1 and Ω_3. For these cases, we have checked condition (15) with the convex relaxation approach discussed in Remark 3. More precisely, for the analysis we consider $u_1 \in [275, 320]$ (K), $u_2 \in [-0.05, 0.13]$ $(\mathrm{kg/m^3/s})$, $x_1 \in [0.05, 2]$ $(\mathrm{kg/m^3})$, $x_2 \in [6360, 6685]$ $(\mathrm{kg/m^3})$ and the parameters presented in Table I. In absorption and desorption scenarios, the constants have been fixed to $\mu = 40$ and $q = 10$. The matrix $\mathbf{P}$ has been selected as

$$\mathbf{P} = \begin{bmatrix} 2 & 1 \\ 1 & 1 \end{bmatrix}, \tag{24}$$

which satisfies

$$\mathbf{P}\frac{\partial \mathbf{f}_1}{\partial \mathbf{x}}(\mathbf{x}, \mathbf{u}) + \frac{\partial \mathbf{f}_1}{\partial \mathbf{x}}(\mathbf{x}, \mathbf{u})^\top \mathbf{P} - \mu \mathbf{c}^\top \mathbf{c} \leq -q\mathbf{P}, \tag{25}$$

$$\mathbf{P}\frac{\partial \mathbf{f}_3}{\partial \mathbf{x}}(\mathbf{x}, \mathbf{u}) + \frac{\partial \mathbf{f}_3}{\partial \mathbf{x}}(\mathbf{x}, \mathbf{u})^\top \mathbf{P} - \mu \mathbf{c}^\top \mathbf{c} \leq -q\mathbf{P}, \tag{26}$$

for the aforementioned sets and parameters.

As a conclusion of this observability analysis, we deduced that, in the considered set of state and input values, the following structural properties can be inferred for the MH tank model (1):

$$\begin{cases} \Omega_1: & \text{differentially detectable} \\ \Omega_2: & \text{non-expansive} \\ \Omega_3: & \text{differentially detectable} \end{cases} \tag{27}$$

We highlight that the system (1) does not only present the properties in (27), but, all differential and non-expansive properties are satisfied with the same metric $\mathbf{P}$, presented in (24). This fact will be exploited in the following section in order to design the observer.

IV. Observer design of the MH tank model

A. Proposal

In this work, we propose the following observer

$$\dot{\hat{\mathbf{x}}} = \mathbf{f}_\sigma(\hat{\mathbf{x}}, \mathbf{u}) + \frac{\mu}{2}\mathbf{P}^{-1}\mathbf{c}^\top(y - \mathbf{c}\hat{\mathbf{x}}), \tag{28}$$

where $\mathbf{f}_\sigma$ is the piecewise defined vector field, μ and the metric $\mathbf{P}$ are defined in (24). A major assumption for the proposed observer (28) is that the switching signal σ in the vector field $\mathbf{f}_\sigma$ is the same as the one in (21). In other words, the observer and the MH tank have a synchronized switching. This may be a very strong assumption, considering that part of the state vector is completely unknown. Nonetheless, we offer a strategy for achieving such synchronization in Section IV-B. We remark that the observer feedback term does not switch. Additionally, notice that, from the observer point of view, σ is a time-varying signal which we will define here as $\sigma : [t_0, \infty) \to \mathcal{G}$. In other words, while the system (21) has a state/input-dependant switching, observer (28) has a time-dependant switching.

It should be noted that even if the observer and the plant have a synchronized switching, the estimation error may not satisfy the convergence property in (12) for all the operating region. This is a consequence of the region Ω_2, where the system only satisfies a non-expansive property and does not satisfy any kind of observability/detectability analysis. This fact is formalized through a Lyapunov argument in the following lemma.

Lemma 1: Consider system (21)*, observer* (28) *and assume that conditions* (25) *and* (26) *hold for some matrix* $\mathbf{P} = \mathbf{P}^\top > 0$ *and positive constants* $\mu > 0, q > 0$*. Additionally, assume that* $\hat{\boldsymbol{x}}(t) \in \mathcal{X}$ *for all* $t \geq 0$*. Then, for each mode* $i \in \mathcal{G}$*, the Lyapunov function of the form* $V_i = (\mathbf{x} - \hat{\mathbf{x}})^\top \mathbf{P}(\mathbf{x} - \hat{\mathbf{x}})$ *such that, for all* $(\mathbf{x}, \mathbf{u}) \in \Omega_i$ *and all* $(\hat{\mathbf{x}}, \mathbf{u}) \in \Omega_i$*, we have*

$$\dot{V}_1 \leq -qV_1, \quad \dot{V}_2 \leq 0, \quad \dot{V}_3 \leq -qV_3. \tag{29}$$

The proof of Lemma 1 is postponed to Appendix A.

In other words, since we are in the constant metric case, observer (28) is contractive, according to Definition 3, during the absorption or desorption processes, while its non-expansive, according to Definition 2, during the equilibrium process. Consequently, there may be scenarios where the observer does not present the convergence property (12). That is the case, for instance, when the system is always at equilibrium and $\sigma(t) = 2\ \forall t \geq 0$. Indeed, Lemma 1 by itself (and considering that $V_1 = V_2 = V_3$) only shows that the estimation error $\mathbf{x} - \hat{\mathbf{x}}$ is bounded, but not that is exponentially convergent. Nonetheless, during the absorption and desorption processes, the observer does present the convergence property (12). Therefore, if system (21) remains in the observable modes for a sufficiently long time, convergence of observer (28) can be guaranteed. This fact is formalized in the following theorem.

Theorem 1: Consider system (21)*, observer* (28) *and assume that conditions* (25) *and* (26) *hold for some matrix* $\mathbf{P} = \mathbf{P}^\top > 0$ *and positive constants* $\mu > 0, q > 0$*. Additionally, assume that* $\hat{\boldsymbol{x}}(t) \in \mathcal{X}$ *for all* $t \geq t_0 \geq 0$*. Moreover, denote* $T_p(t_i, t_{i+1})$ *as the sum of the total time that* $\sigma(t) = p$ *in the interval* $[t_i, t_{i+1})$*. Then, for any switching signal* $\sigma : [t_0, \infty) \to \mathcal{G}$ *and corresponding switching instants:* $\mathfrak{G} \coloneqq \{t_1, t_2, \ldots, t_k, \ldots\}$ *such that*

$$T_1(t_0, t) + T_3(t_0, t) \geq c(t - t_0), \quad \forall t \geq t_0 \tag{30}$$

holds for some constant $0 < c \leq 1$ *and* $t_1 > t_0 \geq 0$*, the switched observer system* (28) *is uniformly contracting according to Definition 3 and the observer error satisfies* (12) *for all* $t \geq t_0 \geq 0$*.*

The proof of this theorem can be found in Appendix B.

Intuitively, (30) implies that the time spend by the MH tank at a absorption or desorption process grows linearly with the total time. We highlight that (30) implies that $\lim_{t\to\infty} T_1(t_0, t) + T_3(t_0, t) = \infty$. Additionally, we remark that the convergence of the observer is independent on the total time spent in the pressure equilibrium mode or the amount of times that the system switches to this mode. This a direct consequence of the fact that the system and the observer are non-expansive in this mode.

B. On synchronizing the switching between the observer and the plant

It is worth noting that observer (28) has to be synchronized to the system mode σ, thus, developing a method to determine the mode of the system is a fundamental part of the algorithm.

We highlight that, based on (3), the mode of the system can be determined by the sign of the value of the normalized sorption mass flow rate f_r. Consequently, if the function f_r can be estimated, then, the estimation, denoted here as $\hat{f}_r$, can be used as a switching signal to tune the observer modes. In other words, we propose the following switching mechanism for the observer:

$$\dot{\hat{\mathbf{x}}} = \begin{cases} \mathbf{f_1}(\hat{\mathbf{x}}, \mathbf{u}) + \frac{\mu}{2}\mathbf{P}^{-1}\mathbf{c}^\top(y - \mathbf{c}\hat{\mathbf{x}}), & \hat{f}_r > \epsilon_{tol}, \\ \mathbf{f_2}(\hat{\mathbf{x}}, \mathbf{u}) + \frac{\mu}{2}\mathbf{P}^{-1}\mathbf{c}^\top(y - \mathbf{c}\hat{\mathbf{x}}), & \left|\hat{f}_r\right| \leq \epsilon_{tol}, \\ \mathbf{f_3}(\hat{\mathbf{x}}, \mathbf{u}) + \frac{\mu}{2}\mathbf{P}^{-1}\mathbf{c}^\top(y - \mathbf{c}\hat{\mathbf{x}}), & \hat{f}_r < -\epsilon_{tol}, \end{cases} \tag{31}$$

where ϵ_{tol} is a positive threshold included to consider potential errors during the estimation of f_r.

Thus, what remains is developing an estimator of the normalized sorption mass flow rate f_r. In this work, we propose using the unknown system dynamics estimator (USDE) proposed in [11]. Precisely, consider the subsystem of (1):

$$\dot{y} = \frac{u_2 - f_r}{v_g}, \tag{32}$$

where y is the density of hydrogen which can be computed as in (19). Assume that the normalized sorption mass flow rate f_r and its derivative are bounded, i.e. $\sup_{s\in[0,\infty)}|\dot{f}_r(s)| \leq \lambda_{fr}$ for a positive constant $\lambda_{fr} > 0$. This is a reasonable assumption in MH tank systems, since all the states/inputs of the system are bounded and f_r is a piece-wise smooth function. Moreover, consider the following low-pass filter for the known variables y and measured u_2:

$$\begin{cases} \kappa\dot{u}_{2f} + u_{2f} = u_2, & u_{2f}(0) = 0 \\ \kappa\dot{y}_f + y_f = y, & y_f(0) = 0 \end{cases} \tag{33}$$

where κ is the parameter of the low-pass filter which can be tuned between the robustness and the convergence speed, u_{2f} and y_f are the filtered version of u_2 and y, respectively. Then, we can design an estimator for the normalized sorption mass flow rate f_r as follows:

$$\hat{f}_r = u_{2f} - v_g \cdot \frac{y - y_f}{\kappa}. \tag{34}$$

The convergence of the estimator is formalized in the following theorem.

Theorem 2 ([11]): Consider (32) *and assume that* $\sup_{s\in[0,\infty)}|\dot{f}_r(s)| \leq \lambda_{fr}$ *for a positive constant* $\lambda_{fr} > 0$. *Then, the estimator* (34)*, satisfies for all* $t \geq 0$

$$\|f_r(t) - \hat{f}_r(t)\| \leq \sqrt{e^{-\frac{t}{\kappa}}\|f_r(0) - \hat{f}_r(0)\| + \kappa^2\lambda_{fr}^2}.$$

We highlight that the convergence rate of the estimator can be increased by reducing the parameter κ. Additionally, notice that we have

$$\lim_{t\to\infty} \|f_r(t) - \hat{f}_r(t)\| \leq \kappa\lambda_{fr}. \tag{35}$$

Thus, the estimation error decreases proportionally to the decrease of κ. Considering this, we can see that the threshold in (31) should be selected such that $\epsilon_{tol} > \kappa\lambda_{fr}$ and t_0 in Theorem 1 (the time that the observer starts operating) should be considered sufficiently large such that $e^{-\frac{t_0}{\kappa}}\|f_r(0) - \hat{f}_r(0)\| \approx 0$.

V. Numerical simulations

In this section, two numerical simulations are designed to validate the feasibility of the proposed observation scheme. The first simulation assumes that the initial state of the MH tank is at equilibrium (case I), while the second simulation considers that the tank starts in the absorption phase (case II). In both two case scenarios, the temperature evolution is generated using the thermodynamic model of MH tanks, as detailed in [13]

$$\dot{t}_{tank} = \frac{f_r\frac{\Delta H}{M_{H_2}} + f_r t_{tank}(c_{pg} - c_{ps}) + \frac{k_{amb}\cdot(t_{amb} - t_{tank})}{v_{MH}}}{v_g c_{pg}\rho_g + v_s c_{ps}\rho_s},$$

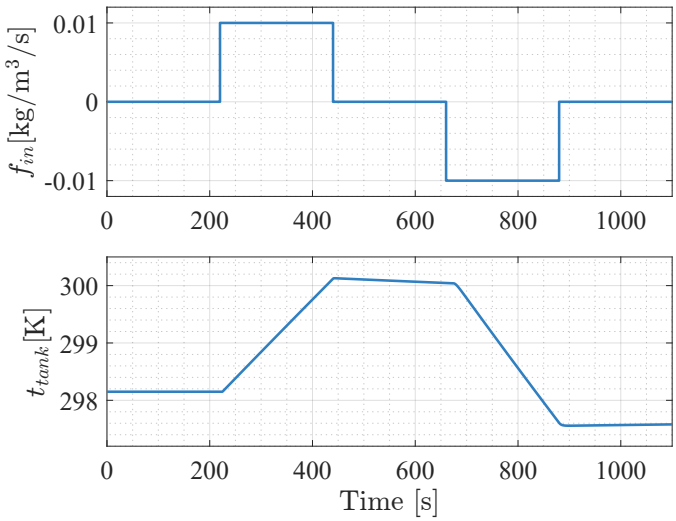

Fig. 2. Evolution of f_{in} and t_{tank} for the system (21) in the simulation Case I.

where c_{pg} and c_{ps} are the specific heat of hydrogen and MH, respectively. k_{amb} is the overall heat exchange coefficient between the ambient air and the MH tank, and t_{amb} is the ambient temperature. The parameters listed in Table I are used, with additional parameters provided in Table II for the thermal model. In both case scenarios, as analyzed in the above section,

Table II: Thermodynamic model and rest parameters.

Symbol	Value	Symbol	Value
ΔH_a	2.072×10^4 J/mol	t_{amb}	298.15 K
c_{pg}	14 890 J/(kg · K)	c_{ps}	6255.4 J/(kg · K)
k_{amb}	0.7485 J/(s · K)	ρ_{si}	6363.7 kg/m^3
k_p	0.8487	m_{total}	0.0315 kg

the observer parameters have been fixed to $\mu = 40$ and $q = 10$. The matrix $\mathbf{P}$ has been selected as

$$\mathbf{P} = \begin{bmatrix} 2 & 1 \\ 1 & 1 \end{bmatrix}, \tag{36}$$

which satisfies the condition in (25) and (26). The low-pass filter parameter κ in (34) is fixed to $\kappa = 1 \cdot 10^{-1}$ and the threshold in (31) is chosen as $\epsilon_{tol} = 1 \cdot 10^{-5}$.

A. Case I

In the first case, we assume that the initial condition of the MH tank is in equilibrium. The system inputs, the normalized mass flow rate, f_{in}, and the tank temperature, t_{tank}, are shown in Fig. 2. Initial value of temperature is $t_{tank}(0) = 298.15$ K. In this case, the system belongs to the non-expansive region in the initial state. The system initial conditions are taken as $x_1(0) = 0.3253$ kg/m^3, $x_2(0) = 6363.7$ kg/m^3, and the observer initial conditions are taken as $\hat{x}_1(0) = 0.6$ kg/m^3, $\hat{x}_2(0) = 6390$ kg/m^3.

The results of the simulation are illustrated in Fig. 3. As observed, the estimation of the sorption rate $\hat{f}_r$ and the estimation $\hat{x}_1$ converge quickly within the first 5s while the estimation $\hat{x}_2$ remains constant at the first 220s and, then,

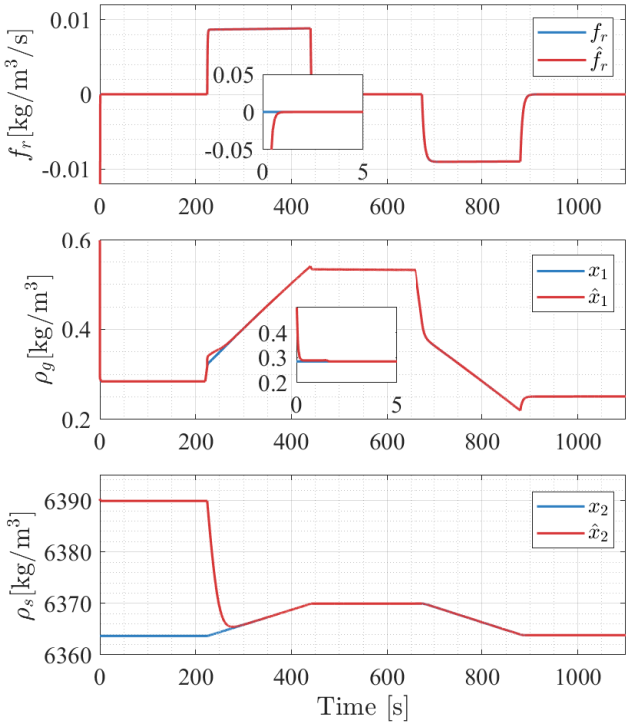

Fig. 3. Comparison of the USDE and observer estimation with true values for the simulation in Case I.

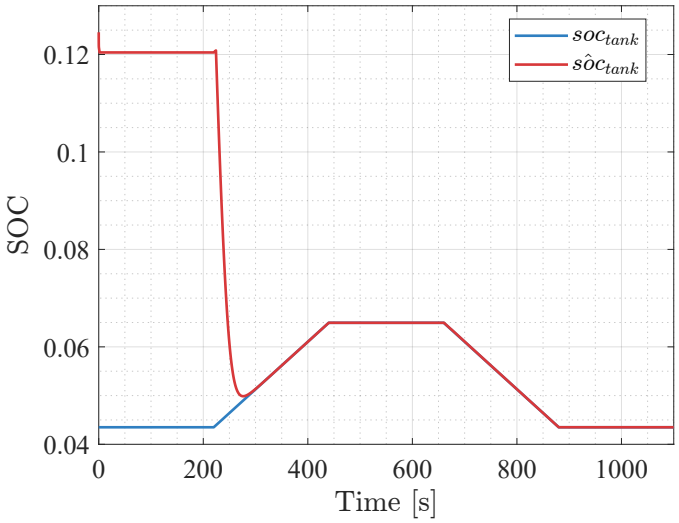

Fig. 4. Comparison of SOC estimation with true values for the simulation in Case I.

converges quickly after 220s, once the system has switched to an observable region.

Finally, the SOC estimation of the MH tank $\hat{soc}_{tank}$ is shown in Fig. 4. It can be found that the estimation of SOC has the same trend as the estimation of x_2.

B. Case II

In the second case, we assume that the initial condition of the MH tank is in an absorption process and switch between charge and discharge within first 100s. The system inputs, the

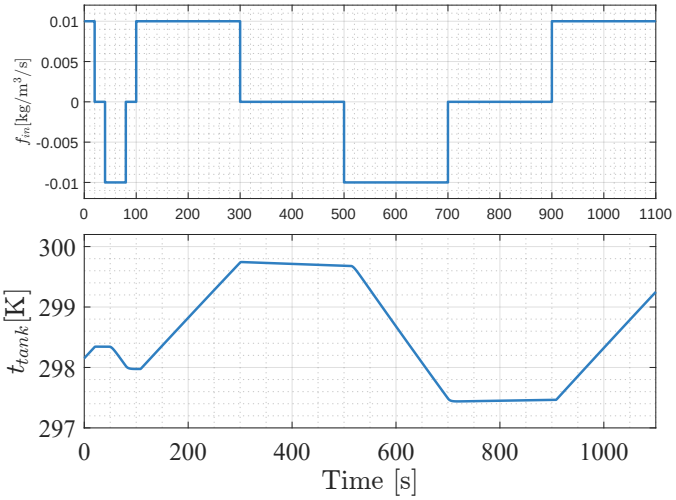

Fig. 5. Evolution of f_{in} and t_{tank} for the system (21) in the simulation Case II.

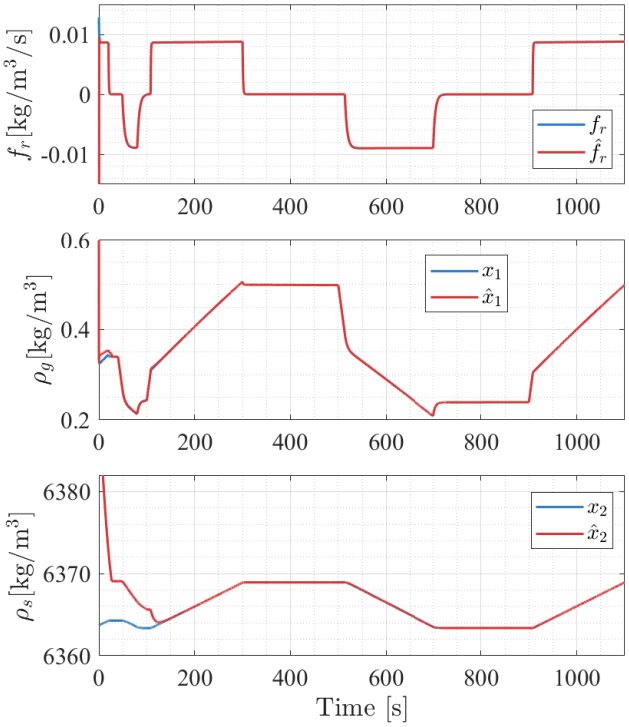

Fig. 6. Comparison of estimator and observer results with true values for the simulation in Case II.

normalized mass flow rate, f_{in}, and the tank temperature, t_{tank}, are shown in Fig. 5. Initial value of temperature is $t_{tank}(0) = 298.15\,\mathrm{K}$. Unlike the first case, in the second case the system belongs to the contractive region in the initial state.

The system initial conditions are taken as $x_1(0) = 0.3253\,\mathrm{kg/m^3}$, $x_2(0) = 6363.7\,\mathrm{kg/m^3}$, and the observer initial conditions are taken as $\hat{x}_1(0) = 0.6\,\mathrm{kg/m^3}$, $\hat{x}_2(0) = 6390\,\mathrm{kg/m^3}$.

The results of the simulation are illustrated in Fig. 6.

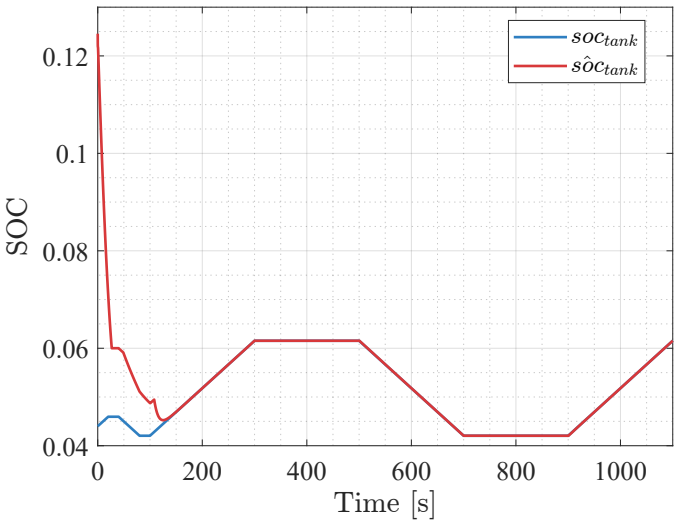

Fig. 7. Comparison of SOC estimation with true values for the simulation in Case II.

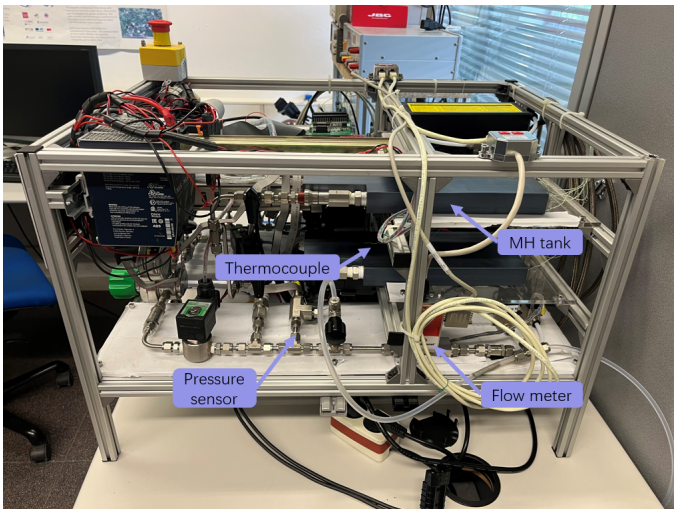

Fig. 8. View of the MH tank test bench environment.

As observed, the estimation of the sorption rate $\hat{f}_r$ and the estimation $\hat{x}_1$ converge in a very short time at the beginning of the stage. Besides, the estimation $\hat{x}_2$ shows a stepwise convergence to x_2 which corresponds to the switching of $\hat{f}_r$ between contractive and non-expansive regions. After 300s, although the system still enters the equilibrium region Ω_2 subsequently, the observation error is still bounded due to the non-expansive property.

The SOC estimation of MH tanks $\hat{soc}_{tank}$ computed as in (13) is shown in Fig. 7.

VI. Experimental Validation

The proposed observer and SOC estimation has been validated in a real experimental setup depicted in Fig. 8. The main components of the setup are a commercial MH tank (H2planet® MyH2 SLIM 350), several mass flow meters (F-111B), pressure sensors (PR-21Y) and thermocouples. All the sensors are connected to a real-time platform (NI sbRIO 9629) to store and process all the data. All the unknown parameters are identified using the same method proposed in [13].

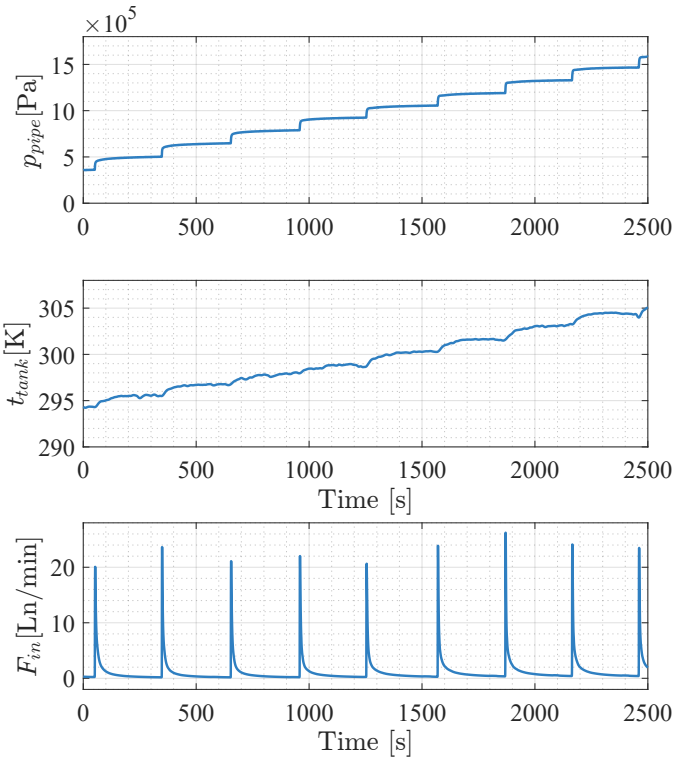

Fig. 9. Experiment measurable variables (charge): pipe pressure p_{pipe}, tank temperature t_{tank} and flow rate F_{in}.

A. Case I

The first experiment is a charging experiment. The pressure is controlled by the pressure regulator and increases gradually in steps. It is important to note that the flow peaks caused by each pressure increase do not exceed the maximum measuring range of the flow meter.

Fig. 9 shows the evolution of measurable variables during the first experiment: pipe pressure p_{pipe}, tank temperature t_{tank} and flow rate F_{in}.

The low-pass filter parameter κ in (34) is fixed to $\kappa = 1$ and the threshold in (31) is chosen as $\epsilon_{tol} = 1 \cdot 10^{-5}$. To verify the designed observer can converge with different initial values, we set two different initial conditions corresponding to the cases of absorption and desorption. The initial conditions of the observer for absorption are taken as $\hat{x}_1(0) = 1\,\mathrm{kg/m^3}$, $\hat{x}_{2,ab}(0) = 6400\,\mathrm{kg/m^3}$ and the initial conditions for desorption are taken as $\hat{x}_1(0) = 1\,\mathrm{kg/m^3}$, $\hat{x}_{2,de}(0) = 6355\,\mathrm{kg/m^3}$. The observer parameters have been fixed to $\mu = 40$ and $\mathbf{P} = \begin{bmatrix} 2 & 1 \\ 1 & 1 \end{bmatrix}$. Fig. 10 shows the results of the estimator (34). Since the true value of f_r cannot be measured directly, here we use f_{in} for comparison. Indeed, since the total mass is conserved, the evolution of f_{in} and f_r should be very similar during the transients and the same value at steady-state. It can be seen that the designed USDE is able to track the evolution of f_{in} well. However, it is particularly noteworthy that the error between $\hat{f}_r$ and f_r is related to the derivative of f_r

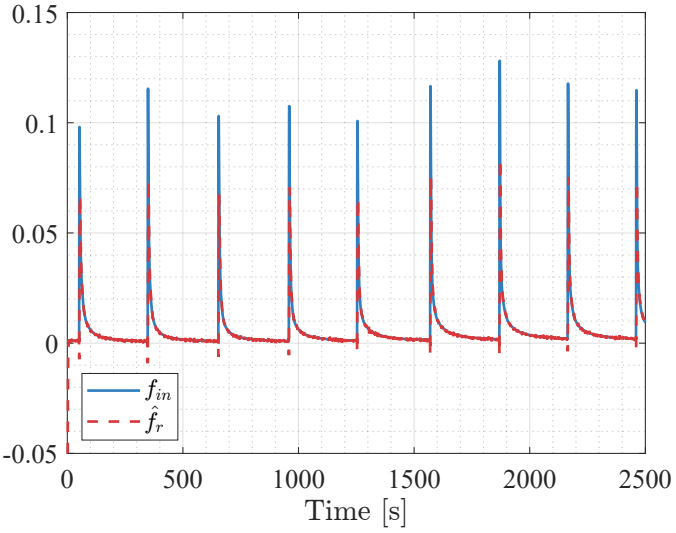

Fig. 10. Estimator results obtained for the experimental results (charge).

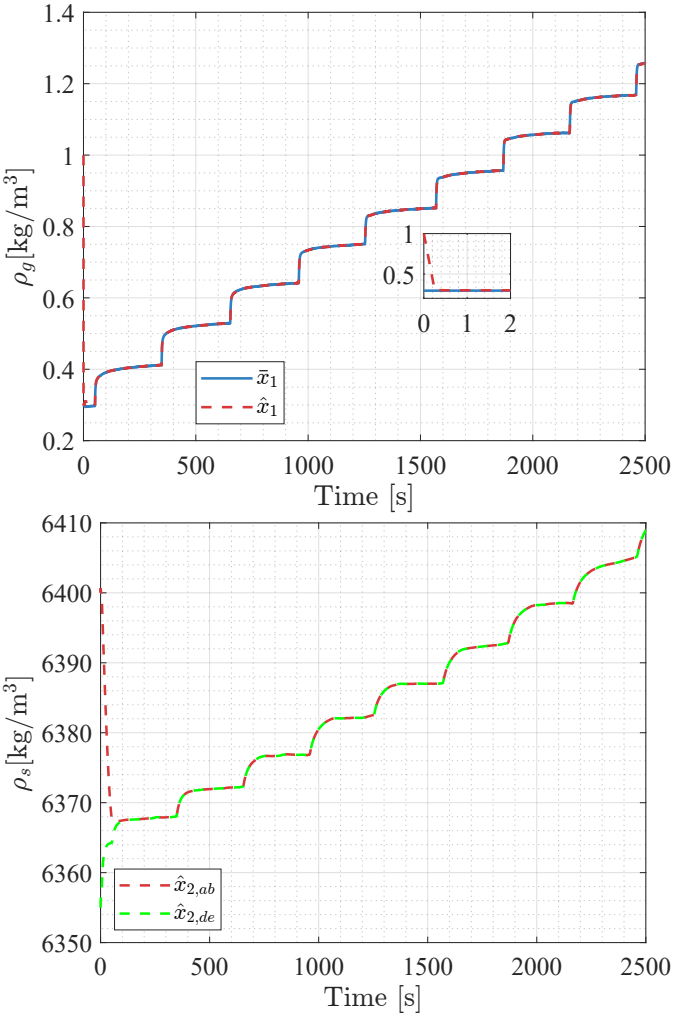

Fig. 11. Observer results obtained for the experimental results (charge).

according to (IV-B). For instance, at around 350s, there exists error in the estimate of f_r due to the large derivative, so the value of $\hat{f}_r$ changes from positive to negative and the observer mode switches directly from region Ω_1 to region Ω_3 based on observer mode switching mechanism (31). This transient error causes small periods of non-synchronization between the observer and the system. Nonetheless, this sporadic non synchronization does not have any apparent effect on the estimation. Fig. 11 shows the evolution of the estimation of ρ_g. The estimation $\hat{x}_1$ converges within 1s. It is important to emphasize that $\bar{x}_1$ is directly calculated from the measurable pressure and temperature signals, making it highly sensitive to measurement noise. In contrast, $\hat{x}_1$ exhibits a smoother profile compared to $\bar{x}_1$. Additionally, Fig. 11 also shows the evolution of the estimation of ρ_s with different initial conditions.

Finally, Fig. 12 shows the evolution of the SOC estimation, $\hat{soc}_{tank,ab}$ and $\hat{soc}_{tank,de}$. Since it is computed from $\hat{x}_1$ and $\hat{x}_2$, the convergence time depends on the convergence time of both $\hat{x}_1$ and $\hat{x}_2$. The equation (8) has been used to obtain an approximation of soc_{tank} as the true value cannot be directly measured. It should be noted that since the initial soc_{tank}, $m_{H_2}(0)$, is unknown, a posteriori value, α, has been estimated from the PCT curve (given by the providers of the MH tank) at equilibrium pressure. We highlight that approximate calculation of soc_{tank} can only be done off-line when all the data is available, while the proposed observer can be implemented on-line. As it can be seen from the figure that $\hat{soc}_{tank,ab}$ and $\hat{soc}_{tank,de}$ converge to soc_{tank} within 100s which shows the effectiveness of the proposed SOC estimation framework.

B. Case II

The second experiment is a discharging experiment. In discharging process, the valve of the discharge pipeline is opened to keep the flow rate steady.

Fig. 13 shows the evolution of measurable variables during the second experiment: pipe pressure p_{pipe}, tank temperature t_{tank} and flow rate F_{in}.

Similar to the first experiment, two different initial conditions are set. The initial conditions of the observer for absorption are taken as $\hat{x}_1(0) = 1\,\mathrm{kg/m^3}$, $\hat{x}_{2,ab}(0) = 6560\,\mathrm{kg/m^3}$ and the initial conditions for desorption are taken as $\hat{x}_1(0) = 1\,\mathrm{kg/m^3}$, $\hat{x}_{2,de}(0) = 6410\,\mathrm{kg/m^3}$. While the other parameters are the same as in Case I. Fig. 14 shows the results of the estimator (34). It can be seen that the designed USDE, after some transient, is able to track the evolution of f_{in} well. Fig. 15 shows the evolution of the estimation of ρ_g and ρ_s. The estimation $\hat{x}_1$ converges within 1s.

Finally, Fig. 16 shows the evolution of the SOC estimation, $\hat{soc}_{tank}$. As it can be seen from the figure that $\hat{soc}_{tank,ab}$ and $\hat{soc}_{tank,de}$ converge to soc_{tank} within 800s which also shows the effectiveness of the proposed SOC estimation framework. The factor soc_{tank} has been computed following the same procedure as in the previous section.

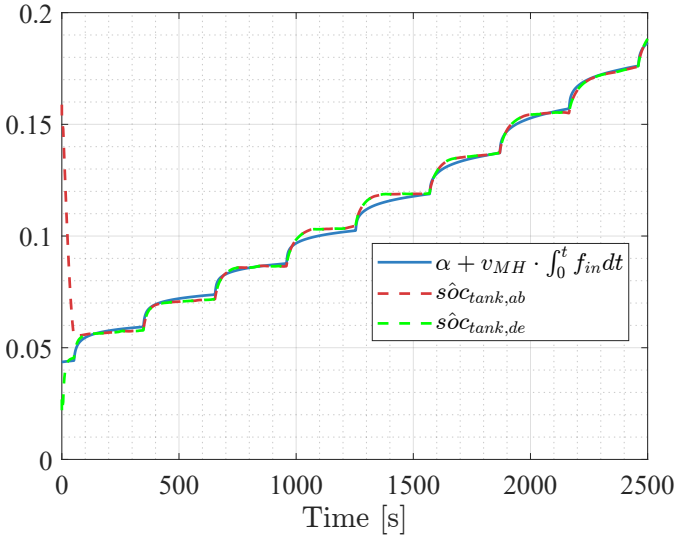

Fig. 12. SOC estimation : comparison between the observer estimation and an offline estimation (charge).

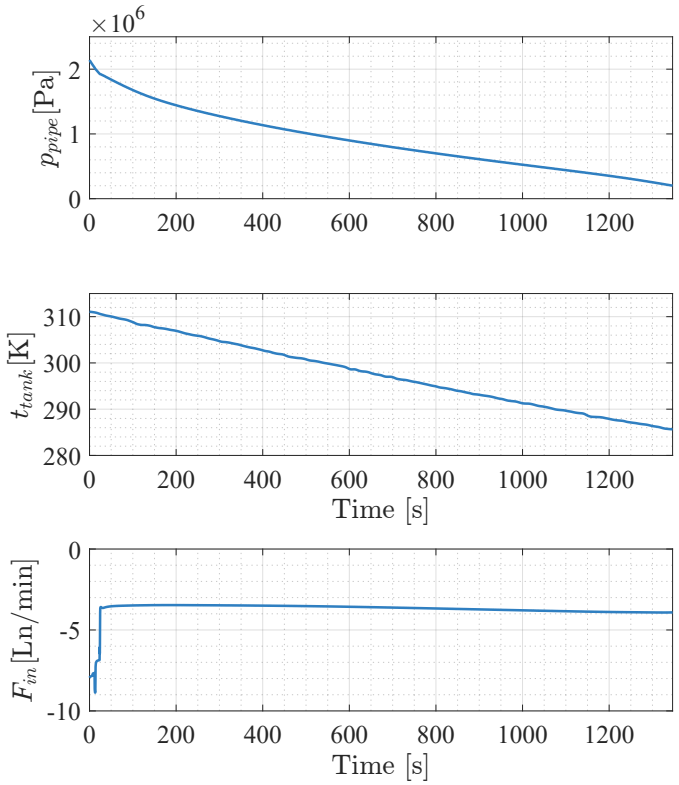

Fig. 13. Experiment measurable variables (discharge): pipe pressure p_{pipe}, tank temperature t_{tank} and flow rate F_{in}.

VII. Conclusion

This work has presented a nonlinear observer for estimating the density of hydrogen and metal hydride in the MH tank to further estimate the SOC of the MH tank. It has been demonstrated that the MH tank dynamics satisfy the differential detectability property with respect to an Euclidean metric in some operating regions and a non-expansive property in some other. These properties have been used to design a nonlinear switched observer. Furthermore, it has been shown that under some switching conditions, the switched observer, synchronised with the system, is uniformly contracting. The proposed observer and SOC estimation framework has been validated through two numerical simulations and in a practical setup.

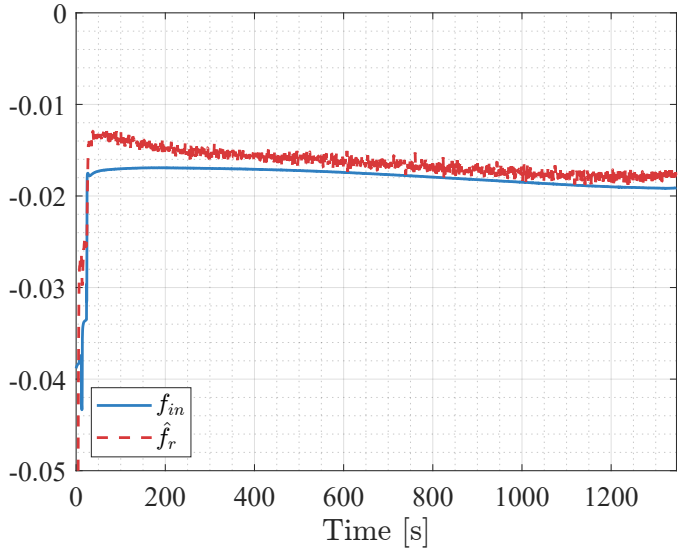

Fig. 14. Estimator results obtained for the experimental results (discharge).

Appendix A
Proof of Lemma 1

Denote $\tilde{\mathbf{x}} = \mathbf{x} - \hat{\mathbf{x}}$. Then, since $\mathbf{f}_i$ is a C^1 function for all $i \in \mathcal{G}$, we have the following identify for all $i \in \mathcal{G}$

$$\mathbf{f}_i(\mathbf{x},\mathbf{u}) - \mathbf{f}_i(\hat{\mathbf{x}},\mathbf{u}) = \left(\int_0^1 \frac{\partial \mathbf{f}_i}{\partial \mathbf{x}}(\hat{\mathbf{x}} + s\tilde{\mathbf{x}}, \mathbf{u}) ds \right) \tilde{\mathbf{x}} \tag{37}$$

for all $(\mathbf{x},\mathbf{u}) \in \Omega_i$ and $(\hat{\mathbf{x}},\mathbf{u}) \in \Omega_i$. With this identity in mind, we will begin by proving the first inequality in (29). Differentiating V_1 and using the identity in (37) we obtain for all $(\mathbf{x},\mathbf{u}) \in \Omega_1$ and $(\hat{\mathbf{x}},\mathbf{u}) \in \Omega_1$

$$\begin{aligned}
\dot{V}_1 &= 2\tilde{\mathbf{x}}^\top \mathbf{P} \left(\mathbf{f}_1(\mathbf{x},\mathbf{u}) - \mathbf{f}_1(\hat{\mathbf{x}},\mathbf{u}) - \frac{\mu}{2} \mathbf{P}^{-1} \mathbf{c}^\top \mathbf{C} \tilde{\mathbf{x}} \right) \\
&= 2\tilde{\mathbf{x}}^\top \mathbf{P} \left(\int_0^1 \frac{\partial \mathbf{f}_1}{\partial \mathbf{x}}(\hat{\mathbf{x}} + s\tilde{\mathbf{x}}, \mathbf{u}) ds - \frac{\mu}{2} \mathbf{P}^{-1} \mathbf{c}^\top \mathbf{c} \right) \tilde{\mathbf{x}} \\
&= \tilde{\mathbf{x}}^\top \left[\int_0^1 \left(\mathbf{P} \frac{\partial \mathbf{f}_1}{\partial \mathbf{x}} + \frac{\partial \mathbf{f}_1}{\partial \mathbf{x}}^\top \mathbf{P} - \mu \mathbf{P}^{-1} \mathbf{c}^\top \mathbf{c} \right) ds \right] \tilde{\mathbf{x}} \\
&\leq -q V_1 \,,
\end{aligned}$$

where the last inequality comes from (25). The other inequalities can be proven in a similar manner.

Appendix B
Proof of Theorem 1

This proof is inspired by the developments in [12]. More precisely, starting from the switched observer (28), we con-

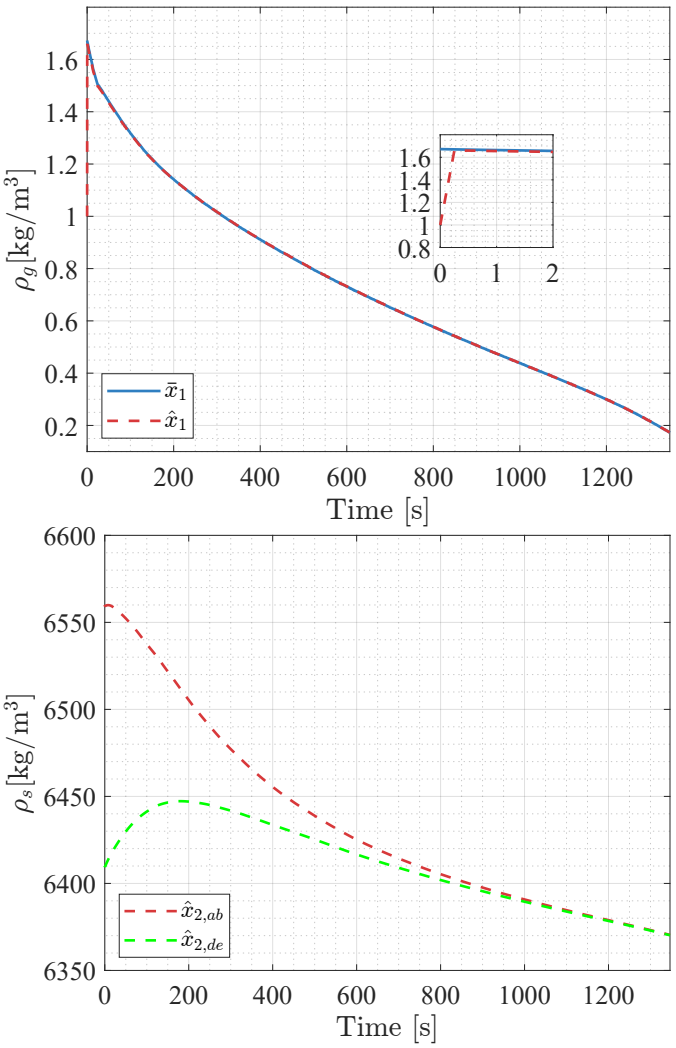

Fig. 15. Observer results obtained for the experimental results (discharge).

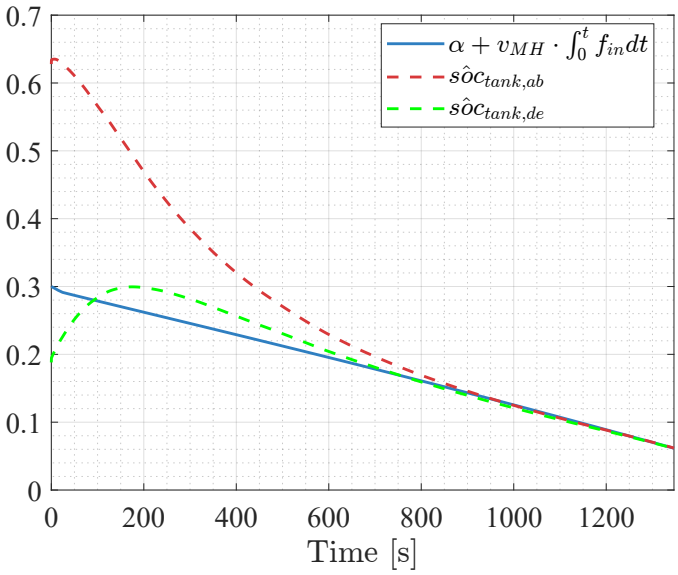

Fig. 16. SOC estimation : comparison between the observer estimation and an offline estimation (discharge).

sider the following family of time-varying linear switched systems for all $p \in \mathcal{G}$:

$$\dot{\boldsymbol{\xi}} = \frac{\partial \mathbf{F}_p}{\partial \hat{\mathbf{x}}}(\hat{\mathbf{x}}, y, \mathbf{u})\boldsymbol{\xi} = \left(\frac{\partial \mathbf{f}_p}{\partial \mathbf{x}}(\hat{\mathbf{x}}, \mathbf{u}) - \frac{1}{2}\mu \mathbf{P}^{-1}\mathbf{c}^\top \mathbf{c}\right)\boldsymbol{\xi}, \quad (38)$$

where $\boldsymbol{\xi} \in \mathbb{R}^2$, $\hat{\mathbf{x}} \in \mathcal{X}$, $\mathbf{u} \in \mathcal{U}$ and $y \in \mathbb{R}$. The first part of the proof consists in showing that, if the switching signal satisfies the time condition (30), the system (38) is uniformly globally exponentially stable.

To do so, first, define the set of Lyapunov functions $V_p(\boldsymbol{\xi}) = \boldsymbol{\xi}^\top \mathbf{P}\boldsymbol{\xi}$ for all $p \in \mathcal{G}$, where $\mathbf{P}$ is defined in (24). Now considering the dynamics (38), equation (23) and the inequalities (25) and (26), repeating the same computations as in Lemma 1 proof shows that,

$$\dot{V}_1(\boldsymbol{\xi}) \leq -qV_1, \quad \dot{V}_2(\boldsymbol{\xi}) \leq 0, \quad \dot{V}_3(\boldsymbol{\xi}) \leq -qV_3. \quad (39)$$

Since the function V_p is fundamentally the same for all $p \in \mathcal{G}$, for all $\boldsymbol{\xi} \in \mathbb{R}^2$

$$V_{\sigma(t_i)}(\boldsymbol{\xi}(t_i)) = V_{\sigma(t_{i-1})}(\boldsymbol{\xi}(t_i)), \quad \forall t_i \in \mathfrak{G} \setminus t_0. \quad (40)$$

Then, for any $t \in [t_{i-1}, t_i)$ and $p = \sigma(t_{i-1})$,

$$\frac{d}{dt}V_p(\boldsymbol{\xi}) = \dot{V}_p(\boldsymbol{\xi}).$$

Therefore, in view of (39) and (40), for any $t \in [t_{i-1}, t_i)$, we have

$$\begin{aligned} V_{\sigma(t_i)}(\boldsymbol{\xi}(t_i)) &= V_{\sigma(t_{i-1})}(\boldsymbol{\xi}(t_i)) \\ &\leq e^{q_p(t_i - t_{i-1})} V_{\sigma(t_{i-1})}(\boldsymbol{\xi}(t_{i-1})), \end{aligned}$$

where we defined $q_1 = q_3 = q$ and $q_2 = 0$. Additionally, by applying recursively this inequality we get for any $t \in [t_i, t_{i+1})$,

$$V_{\sigma(t_i)}(\boldsymbol{\xi}(t)) \leq c_\sigma(t) V_{\sigma(t_0)}(\boldsymbol{\xi}(t_0)) \quad (41)$$

with

$$\begin{aligned} c_\sigma(t) &= e^{q_p(t-t_i)} \prod_{k=0}^{i-1} e^{q_p(t_{k+1}-t_k)} = \prod_{p \in \mathcal{G}} e^{q_p T_p(t_0,t)} \\ &= e^{-q_1 \cdot T_1(t_0,t) + 0 \cdot T_2(t_0,t) - q_3 \cdot T_3(t_0,t)} \\ &\leq e^{-q(T_1(t_0,t)+T_3(t_0,t))} \leq e^{-qc(t-t_0)} \end{aligned}$$

where we used the condition (30) in the last line.

Furthermore, since the considered Lyapunov functions satisfy, for all $p \in \mathcal{G}$,

$$\lambda_{min}(\mathbf{P})\|\boldsymbol{\xi}\|^2 \leq V_p(\boldsymbol{\xi}) \leq \lambda_{max}(\mathbf{P})\|\boldsymbol{\xi}\|^2, \quad (42)$$

where $\lambda_{min}(\cdot)$ and $\lambda_{max}(\cdot)$ are minimum and maximum eigenvalue of the matrix, respectively, we have that, for all $t \in [t_i, t_{i+1})$,

$$\begin{aligned} \|\boldsymbol{\xi}(t)\| &\leq \frac{1}{\sqrt{\lambda_{min}(\mathbf{P})}} V_{\sigma(t_i)}^{\frac{1}{2}}(\boldsymbol{\xi}(t)) \\ &\leq \sqrt{\frac{1}{\lambda_{min}(\mathbf{P})}} e^{-\frac{qc}{2}(t-t_0)} V_{\sigma(t_0)}^{\frac{1}{2}}(\boldsymbol{\xi}(t_0)) \quad (43) \\ &\leq \sqrt{\frac{\lambda_{max}(\mathbf{P})}{\lambda_{min}(\mathbf{P})}} e^{-\frac{qc}{2}(t-t_0)} \|\boldsymbol{\xi}(t_0)\|, \end{aligned}$$

which shows that (38) is uniformly globally exponentially stable if (30) holds.

Now by means of [12, Proposition 3.1], since (38) is uniformly globally exponentially stable we have that observer (28) is contractive uniformly on the input according to Definition 3. That is, for any input $\mathbf{u} \in \mathcal{U}$ and every two trajectories of observer (28), denoted as $\hat{\mathbf{x}}(t)$, $\hat{\mathbf{x}}'(t)$ in $\mathbf{X}$, there exists some constants $a, b > 0$ such that,

$$\|\hat{\mathbf{x}}(t) - \hat{\mathbf{x}}'(t)\| \leq ae^{-bt}\|\hat{\mathbf{x}}(t_0) - \hat{\mathbf{x}}'(t_0)\|. \tag{44}$$

Finally, considering that the switching signal σ is the same for the plant (28) and observer (28), we get that $\hat{\mathbf{x}}(t) = \mathbf{x}(t)$ for all $t \geq t_0$ is a solution of observer (28). Thus, we conclude that (44) implies (12), which ends the proof.

REFERENCES

[1] C. Tarhan and M. A. Çil, "A study on hydrogen, the clean energy of the future: Hydrogen storage methods," *Journal of Energy Storage*, vol. 40, p. 102676, 2021. I

[2] R. Moliner-Heredia, C. Vivas, and F. R. Rubio, "Gestión óptima en microrredes con soporte fotovoltaico e hidrógeno verde," *Revista Iberoamericana de Automática e Informática industrial*, oct. 2024. [Online]. Available: https://polipapers.upv.es/index.php/RIAI/article/view/21922 I

[3] J. Liu, F. Yang, Z. Wu, and Z. Zhang, "A hybrid modeling method of metal hydride tank and dynamic characteristic analysis," *International Journal of Hydrogen Energy*, vol. 50, pp. 799–811, 2024. I

[4] D. Gehring, M. Kölbig, S. Göltz, J. Heidingsfeld, A. Rentz, O. Sawodny, M. Linder, and I. Bürger, "Metal hydride reactor for output temperature control," *International Journal of Hydrogen Energy*, vol. 50, pp. 1502–1517, 2024. I

[5] A. L. J. Keow, A. Mayhall, M. Cescon, and Z. Chen, "Active disturbance rejection control of metal hydride hydrogen storage," *International Journal of Hydrogen Energy*, vol. 46, no. 1, pp. 837–851, 2021. I

[6] S. Suarez, D. Chabane, A. N'Diaye, Y. Ait-Amirat, and A. Djerdir, "Static and dynamic characterization of metal hydride tanks for energy management applications," *Renewable Energy*, vol. 191, pp. 59–70, 2022. I

[7] D. Chabane, L. Serairi, M. Iqbal, A. Djerdir, N. Fenineche, and O. Elkedim, "Innovative method to estimate state of charge of the hydride hydrogen tank: application of fuel cell electric vehicles," *International Journal of Modelling and Simulation*, vol. 2021, pp. 1 891 495–14, 2021. I

[8] D. Zhu, Y. Ait-Amirat, A. N'Diaye, and A. Djerdir, "On-line state of charge estimation of embedded metal hydride hydrogen storage tank based on state classification," *Journal of Energy Storage*, vol. 42, p. 102950, 2021. I, II-B

[9] F. Gonzatti, M. Miotto, and F. Farret, "Automation and analysis of the operation of (la0. 85ce0. 15) ni5 in energy storage plants," *International Journal of Hydrogen Energy*, vol. 43, no. 5, pp. 2850–2860, 2018. I

[10] P. Bernard, V. Andrieu, and D. Astolfi, "Observer design for continuous-time dynamical systems," *Annual Reviews in Control*, vol. 53, pp. 224–248, 2022. 1, 1, III-A

[11] J. Na, B. Jing, Y. Huang, G. Gao, and C. Zhang, "Unknown system dynamics estimator for motion control of nonlinear robotic systems," *IEEE Transactions on Industrial Electronics*, vol. 67, no. 5, pp. 3850–3859, 2019. 2, IV-B, 2

[12] H. Yin, B. Jayawardhana, and S. Trenn, "On contraction analysis of switched systems with mixed contracting-noncontracting modes via mode-dependent average dwell time," *IEEE Transactions on Automatic Control*, vol. 68, no. 10, pp. 6409–6416, 2023. 2, B, B

[13] M. Chen, C. Batlle, B. Escachx, R. Costa-Castelló, and J. Na, "Sensitivity analysis and calibration for a two-dimensional state-space model of metal hydride storage tanks based on experimental data," *Journal of Energy Storage*, vol. 94, p. 112316, 2024. II-A, V, VI

[14] P. Bernard, N. Mimmo, and L. Marconi, "On the semi-global stability of an ek-like filter," *IEEE Control Systems Letters*, vol. 5, no. 5, pp. 1771–1776, 2021. 2

[15] A. Duvall and E. D. Sontag, "A remark on omega limit sets for non-expansive dynamics," 2024. [Online]. Available: https://arxiv.org/abs/2404.02352 III-A, III-A

[16] F. Bullo, "Contraction theory for dynamical systems," *Kindle Direct Publishing*, 2024. III-A

[17] S. Boyd, L. El Ghaoui, E. Feron, and V. Balakrishnan, *Linear matrix inequalities in system and control theory*. SIAM, 1994. 3